

# Determination of branching ratios for Higgs to di-jet states and WW-fusion fraction at the ILC at $\sqrt{s} = 250$ GeV

Bachelor-Arbeit  
zur Erlangung des Hochschulgrades  
Bachelor of Science  
im Bachelor-Studiengang Physik

vorgelegt von

CHRISTIAN DREWS  
geboren am 18.12.1989 in WISMAR

Institut für Kern- und Teilchenphysik  
Fachrichtung Physik  
Fakultät Mathematik und Naturwissenschaften  
Technische Universität Dresden  
2014

Eingereicht am 09. Juli 2014

1. Gutachter: Jun.-Prof. Dr. Arno Straessner
2. Gutachter: Prof. Dr. Hitoshi Yamamoto

---

## Summary

### Abstract

After the discovery of the Higgs boson in 2012 at the LHC it will be an important task for the International Linear Collider to make precise measurements of its properties to test the Standard Model. This work shows an estimation of the accuracies for the branching ratios  $BR(H \rightarrow b\bar{b}, c\bar{c}, gg)$  in the  $e^-e^+ \rightarrow \nu\bar{\nu}h$  channel. An additional attempt to separate WW-fusion, Higgs-Strahlung and their interference is given. In this study the Higgs mass is assumed to be 125 GeV which leads to a cross section of  $\sigma(e^+e^- \rightarrow \nu\nu H) = 77.53$  fb with a beam polarization of  $P(e^-, e^+) = (-80\%, 30\%)$  further an integrated luminosity of  $250 \text{ fb}^{-1}$  is promised. Furthermore, the influence of hadronic beam-background ( $\gamma\gamma \rightarrow q\bar{q}$ ) on the branching ratio measurements at a mean of 0, 0.2 and 0.4 will be discussed.

### Zusammenfassung

Nach der Entdeckung des Higgsbosons in Jahr 2012 am LHC ist es eine wichtige Aufgabe des Internationalen Linear Collider präzise Messungen der Eigenschaften dieses Teilchen zu machen. In dieser Arbeit soll die Genauigkeit des Verzweungsverhältnisses  $BR(H \rightarrow b\bar{b}, c\bar{c}, gg)$  im  $e^-e^+ \rightarrow \nu\bar{\nu}h$  Kanal bestimmt werden. Diese Arbeit schlägt eine mögliche Herangehensweise zur Separation von WW-Fusion, Higgs-Strahlung und ihre Interferenz vor. Dafür wird in dieser Studie die Higgsmasse als 125 GeV, eine Beampolarisation von  $P(e^-, e^+) = (-80\%, 30\%)$  und eine integrierte Intensität von  $250 \text{ fb}^{-1}$  angenommen. Dies führt zu einem Wirkungsquerschnitt von  $\sigma(e^+e^- \rightarrow \nu\nu H) = 77.53$  fb. Außerdem wird der Einfluss des hadronischen Beam-Hintergrund ( $\gamma\gamma \rightarrow q\bar{q}$ ) für einen Mittelwert von 0, 0.2 und 0.4 auf die Messung des Verzweungsverhältnisses diskutiert.

*Dedication:*

*I am very grateful to Prof. Hitoshi Yamamoto for making this work possible. As to Prof. Arno Straessner for mentoring this work. Thanks also to Junping Tian, Jonas Wilzewski, Sven Brieden, Itaru Ushiki, Shinjiro Yamaguchi, Tomohiro Horiguchi and Shun Watanuki for their support. And last but not least I am especially indebted to Jan Strube for constant supervision and encouragement.*

# Contents

|          |  |           |
|----------|--|-----------|
| <b>1</b> | <b>Introduction</b>                      | <b>1</b>  |
| 1.1      | Motivation . . . . .                     | 1         |
| 1.2      | International Linear Collider . . . . .  | 1         |
| 1.3      | Simulation and Reconstruction . . . . .  | 2         |
| 1.4      | Analysis Strategy . . . . .              | 2         |
| <b>2</b> | <b>Data Analysis</b>                     | <b>3</b>  |
| 2.1      | Event Selection . . . . .                | 3         |
| 2.2      | Branching ratio study . . . . .          | 5         |
| 2.2.1    | Template Fitting . . . . .               | 5         |
| 2.2.2    | TMVA . . . . .                           | 6         |
| 2.3      | T-, S-Channel and Interference . . . . . | 9         |
| 2.4      | Hadronic Beam-Background . . . . .       | 10        |
| <b>3</b> | <b>Summary and Outlook</b>               | <b>13</b> |
| <b>4</b> | <b>Bibliography</b>                      | <b>15</b> |
| <b>A</b> | <b>Appendix</b>                          | <b>17</b> |
| A.1      | Event selection . . . . .                | 17        |
| A.2      | Data Samples . . . . .                   | 22        |
| A.3      | T-, S-Channel and Interference . . . . . | 23        |



# 1 Introduction

## 1.1 Motivation

Since the discovery of the Higgs-boson at the LHC in 2012 ([1], [10]) it has been an important task for modern physics to test the consistency of this new particle with the Standard Model (SM). This study inquires how the SM-like Higgs-boson couplings to gluons, bottom and charm quarks can be observed. These couplings have not been observed so far but precise measurements are important because for different models the couplings to each of the final states can vary. In fact there are many other models such as various Higgs doublet models including supersymmetric versions. These have the potential to answer open questions in modern physics for instance the dark matter abundance, naturalness and the baryon asymmetry of the universe. In the SM all couplings to the Higgs-boson are linear to their mass that has to be tested.

## 1.2 International Linear Collider

The International Linear Collider (ILC) (see figure 1.1) is a proposed electron positron collider based on 1.3 GHz superconducting radio-frequency accelerating technology. The ILC will first operate with center of mass energy in the range of 250 GeV to 500 GeV and can be upgraded to reach up to 1 TeV. At the ILC one needs

few model assumptions, there is few background and it is possible to polarize 80 % of the electron beam and 30 % of the positron beam. The ILC will have two Detectors, the International Linear Detector (ILD) and the Silicon Detector (SiD), which will share the same interaction region by push-pull technique. Here, the focus is on the ILD. It consists of a high-precision vertex detector surrounded by a hybrid tracking system with a silicon tracker and

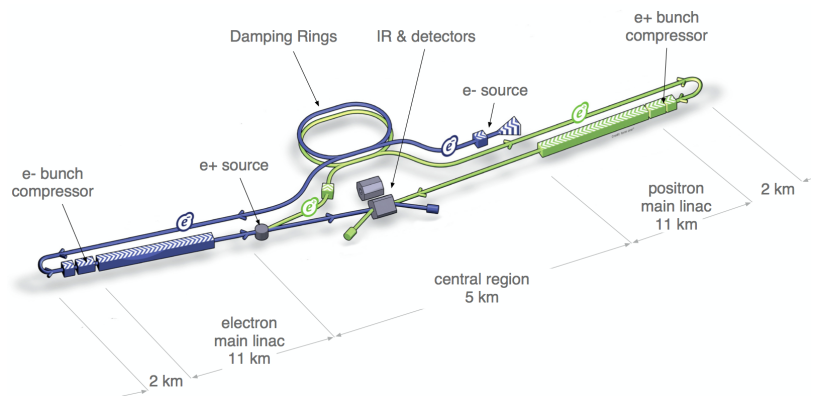


**Figure 1.1:** schematic representation of the ILC [6]

time-projection chamber. For optimal particle-flow performance a highly granular electromagnetic and hadron calorimeter system was developed. The whole detector barrel is contained by a 3.5 T solenoid [6].

### 1.3 Simulation and Reconstruction

In this study Monte Carlo data samples generated by Whizard are analyzed. The detector was simulated with Mokka on a full ILD model based on the Detailed Baseline Design (DBD) [5]. For reconstruction the Pandora Particle Flow Algorithm (PandoraPFA) was used [15], furthermore the LCFIplus package was used for vertex reconstruction and flavor tagging. Marlin [17] and ROOT [3] were used to analyze the simulated data. In the following signal refers to  $e^-e^+ \rightarrow \nu\bar{\nu}h$  where h decays in to  $b\bar{b}$ ,  $c\bar{c}$  or  $gg$  (see Figure 1.2). Only SM processes are considered as Background including various Z, W and Higgs events in leptonic, semileptonic and hadronic final states. Beam photon interactions, which include  $\gamma\gamma$ -annihilation and interactions with beam electrons or positrons were also analyzed. A detailed list of data samples can be found in Table A.4.

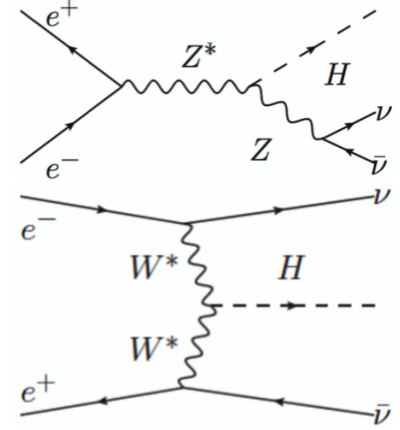


**Figure 1.2:** Feynman diagram of signal, upper WW-fusion, lower Higgs-Strahlung

### 1.4 Analysis Strategy

All data samples are scaled to a polarization of  $P(e^-, e^+) = (-80\%, 30\%)$ , the cross section of the corresponding event and an integrated luminosity of  $\mathcal{L} = 250 \text{ fb}^{-1}$ . This calls for three years running with 100 working days at 250 GeV. All events will be clustered to two jets by the JetClustering algorithm of LCFIplus package (improved version of LCFIVertex package [4]). Further, the jets are tagged with a bottom and a charm quark likeness by the same package. These so called b- and c-tags are computed by reconstructed information about the jets mainly from the vertex detector and the tracking of charged particles to distinguish heavy flavor (c, b) jets from light flavor (u, d, s) jets. In this analysis the b-tags and c-tags are used to compute the  $h \rightarrow b\bar{b}/c\bar{c}$  likeness by  $X = \frac{x_1 + x_2}{2}$ , where  $x_i$  is the flavor-tag of the two jets ( $i = 1, 2$ ). A definition of this value as  $X = \frac{x_1 \cdot x_2}{x_1 \cdot x_2 + (1-x_1) \cdot (1-x_2)}$  (used in [14]) was tested but discarded because of its lower efficiency. The Higgs-boson is reconstructed from the jets and the recoil mass peaks at the mass of the Z-boson in signal events. After selecting the signal (see chapter 2.1) the final states of the Higgs decay will be selected by fitting b- and c-likeness. This strategy was adopted from previous studies ([14], [11]).



# 2 Data Analysis

## 2.1 Event Selection

The cuts were optimized by maximizing the signal significance  $S = N_{Sig}/\sqrt{N_{Sig} + N_{Bg}}$ . The inverse of the significance is for pure counting experiments the relative statistical uncertainty of the measurable, which means in the case of the here described branching ratio measurement  $\frac{\Delta(\sigma Br)}{\sigma Br} = \frac{1}{S}$ .

To optimize the cut variables a program which varies upper and lower cut limit while finding the cut limit with maximal significance was written. Initially every cut was optimized at the same time but from time to time this lead to over correction so that the significance ended up to be much lower after optimizing. Because of this issue it is better to optimize cut after cut, which takes much longer because it is necessary to loop over all cuts about 3 to 5 times, but this technique is very efficient and does not need any monitoring. To check the importance of the cuts and making sure that cuts do not have negative effect on the significance it is useful to look at cut tables where only one cut is taken away (see Table A.2) rather than cut flow tables (see Table 2.1 or Table A.1). If the cut limit range for optimization is not chosen large enough it has negative effect on the significance. To increase the significance for each of the three

**Table 2.1:** summary of background reduction for optimizing on  $h \rightarrow b\bar{b}, c\bar{c}, gg$  (for more detail see Table A.1)

| cut / event type                                  | $\nu\bar{\nu}h$   | semileptonic      | hadronic          | other SM Bg       | significance | efficiency |
|---|-------------------|-------------------|-------------------|-------------------|--------------|------------|
| Expected  | $1.94 \cdot 10^4$ | $4.60 \cdot 10^6$ | $2.37 \cdot 10^7$ | $4.83 \cdot 10^8$ | 0.592        | 1          |
| isoLepCuts  | $1.76 \cdot 10^4$ | $1.78 \cdot 10^6$ | $2.34 \cdot 10^7$ | $3.36 \cdot 10^8$ | 0.697        | 0.992      |
| $N_{PFO,1} > 20$ and $N_{PFO,2} > 11$             | $1.47 \cdot 10^4$ | $8.48 \cdot 10^5$ | $1.62 \cdot 10^7$ | $2.11 \cdot 10^6$ | 2.77         | 0.907      |
| $80 \text{ GeV} < E_{vis} < 147 \text{ GeV}$      | $1.34 \cdot 10^4$ | $4.08 \cdot 10^5$ | $4.91 \cdot 10^6$ | $1.23 \cdot 10^6$ | 4.33         | 0.829      |
| $79.5 \text{ GeV} < M_Z < 131.5 \text{ GeV}$      | $1.20 \cdot 10^4$ | $2.22 \cdot 10^5$ | $8.58 \cdot 10^5$ | $4.55 \cdot 10^5$ | 8.1          | 0.753      |
| $104.5 \text{ GeV} < M_H < 132 \text{ GeV}$       | $1.10 \cdot 10^4$ | $7.16 \cdot 10^4$ | $6.36 \cdot 10^4$ | $1.87 \cdot 10^5$ | 16           | 0.69       |
| $21.5 \text{ GeV} < p_{t,mis} < 67.5 \text{ GeV}$ | 9810              | $5.03 \cdot 10^4$ | 1642              | 2700              | 32.5         | 0.616      |
| $ p_{z,mis}  < 55.5 \text{ GeV}$                  | 9450              | $3.49 \cdot 10^4$ | 1112              | 2400              | 36.3         | 0.594      |
| thrust cuts <sup>1</sup>                          | 7595              | $1.78 \cdot 10^4$ | 972               | 1390              | 41.8         | 0.521      |
| $p_{max,PFO} < 40.5 \text{ GeV}$                  | 7449              | $1.64 \cdot 10^4$ | 914               | 1290              | 42.4         | 0.512      |
| $0.23 < Y_{12} < 0.91$ and $Y_{23} < 0.015$       | 4997              | 3345.2            | 630               | 426               | 50.7         | 0.367      |

final states alone, separate optimization procedures were carried out. Hereby the definition of significance was changed a little bit.  $N_{Sig}$  is the number of the final states that will be

<sup>1</sup>thrust cuts refers to  $0.08 < \text{majthrust} < 0.5$  and  $0.77 < \text{pthrust} < 0.995$  and  $0.521 < \text{minthrust} < 0.35$

optimized while  $N_{Bg}$  stays the number of background. This definition was chosen, because the signal final states can be separated later on with a template fit. However, the other real background increases the uncertainty. Due to the difference in the nature of the jets, the detector resolution and the number of expected events, the separate optimization performed here affects the results. The events from gluons have the best detector resolution, whereas bottom-quark events exhibits the poorest resolution. This can be explained by the relatively large undetectable energy carried away by neutrinos in the bottom jets. This is why the cut on recoil mass is optimized to be looser for events with  $\bar{b}b$  final state. Table A.3 lists all cut variables.  $H \rightarrow bb$  events occur much more frequently compared to the other two considered decay modes. Consequently, the cut variables do not change significantly, if these are the only events under consideration (see Table 2.2).

**Table 2.2:** The number of events selected as signal depending on the optimization for each final state separate

| optimized on                | $h \rightarrow \bar{b}b$ | $h \rightarrow \bar{c}c$ | $h \rightarrow gg$ | $h \rightarrow \bar{b}b, \bar{c}c, gg$ | expected          |
|-----------------------------|--------------------------|--------------------------|--------------------|--|-------------------|
| $N(h \rightarrow \bar{b}b)$ | 4020                     | 1616                     | 991                | 4248                                   | 11100             |
| $N(h \rightarrow \bar{c}c)$ | 180                      | 88                       | 31.71              | 193                                    | 521               |
| $N(h \rightarrow gg)$       | 436                      | 123                      | 455                | 470                                    | 1650              |
| $N(Bg)$                     | 3973                     | 409                      | 652                | 4297                                   | $3.62 \cdot 10^8$ |

In the following the selection cuts are briefly explained:

- isoLepCut refers to a test where events with isolated leptons are rejected. This test is carried out before the actual analysis to reduce the running time of the program. The basic idea of this test is to reject events with leptons with high energy but relatively low energy in the enclosing cone around the leptonic track. This rejects leptonic and semileptonic events. Table 2.1 illustrates the predominance of semileptonic background events. Surprisingly, most of these events are of  $q\bar{q}\ell\nu$  final states (See Table A.1) where these should be rejected by this cut but only two thirds of these events get rejected. Renewed tuning of the rejection maid help enlarge the cut efficiency.
- $N_{PFO}$  is the number of total Particle Flow Objects (PFO) in the event.  $N_{PFO,1}$  and  $N_{PFO,2}$  refer to the number of PFOs in each jet, where  $N_{PFO,1} > N_{PFO,2}$ . Only the PFOs selected by the used FastJetFinder are counted. This cut rejects events without or low energy jets. (see Figure A.3 and A.4)
- $E_{vis}$  is the total visible energy in the Event, which is calculated by summing up over the energies of the PFOs. In this analysis it is the total Higgs energy. The cut on this variable reduces mainly the hadronic and Higgs background, but also the background originating from leptonic and semileptonic events. Only on events with neutrinos it has nearly no effect. (see Figure A.5)

- $p_{max,PFO}$  refers to the maximal momentum of the PFOs. This cut reduces signal and background only a little. However, its influence enhances if we only optimize on gg final states. (see Figure A.13)
- $M_Z$  denotes the recoil mass, which is equivalent to the reconstructed mass of the Z-boson. It is estimated by  $M_Z^2 = ((250 \text{ GeV}/c, \vec{0}) - p_{j,1} - p_{j,2})^2$ , where  $p_{j,i}$  ( $i = 1, 2$ ) is the four-momentum of the two jets. The cut obviously cuts all background, which has no invisible Z-bosons. (see Figure A.1)
- In the same sense  $M_H$  denotes the mass of the Higgs-boson  $M_H^2 = (p_{j,1} + p_{j,2})^2$ . Similar to the cut on the Z-mass this cut reduces all background because of the definition of signal. (see Figure A.2)
- $p_{t,mis}$  is the missing momentum of all added PFOs transversal to the beam pipe.  $p_{z,mis}$  is the corresponding momentum in z-direction. These cuts reduce mainly hadronic backgrounds. (see Figure A.9)
- majthrust, pthrust and minthrust stand for principle, major and minimal thrust, which describe the distribution of reconstructed momentum in the event [8]. In the cut tables these cuts are summarized as thrust. These cut some Higgs backgrounds and backgrounds from ZZ production with only one invisible Z. (see Figure A.6, A.7 and A.8)
- $Y_{12}$  and  $Y_{23}$  are given by the FastJetFinder to discriminate the number of jets in the event [9]. This cut mainly reduces  $q\bar{q}\ell\nu$  final states. (see Figure A.11 and A.12)
- $N_\mu$  refers to the number of particles identified as muon. This cut only reduces semileptonic background in case of gluon final state.

## 2.2 Branching ratio study

### 2.2.1 Template Fitting

The accuracy measurement of branching ratios is performed on the basis of a template fitting with the RooFit package [16]. The b- and c-likeness was fitted in a two dimensional histogram of 20 by 20 bins. The templates were produced from samples of 100,000 events of each final states  $h \rightarrow b\bar{b}$ ,  $c\bar{c}$  and gg while the template for the background was generated from the ordinary samples (see Figure 2.2). The probability of a given number of events in the  $(i, j)$  bin is given by the Poisson-distribution.

$$P_n(\mu) = \frac{e^{-\mu} \mu^n}{n!}$$

Here,  $\mu$  is the number of events in the  $(i, j)$  bin in the template and  $n$  is the number of events in the Data in this bin. To evaluate the fit a toy study was performed. 10,000 data histograms were generated and fitted. The data histograms were generated from each template and added. The results can be found in Figure 2.1. The uncertainty on  $\sigma \cdot BR$  was estimated by the mean of the fitting error of the 10,000 toy fits where  $\sigma$  is the cross section of  $\nu\bar{\nu}h$  production. Further, the relative uncertainty on the Branching ratio is given by

$$\frac{\Delta BR}{BR} = \sqrt{\frac{\Delta N_{fit}^2}{N_{fit}} + \frac{(\epsilon_{WW}\Delta\sigma_{WW}) + (\epsilon_{ZH}\Delta\sigma_{ZH})^2}{(\epsilon_{WW}\sigma_{WW} + \epsilon_{ZH}\sigma_{ZH})^2}}$$

The uncertainty of the cross section of the Higgs-Strahlung  $\sigma_{ZH}$  is determined by the Higgs recoil mass measurement and assumed to be 2.5 % [2].  $\epsilon_{WW} = 0.234$  is the efficiency on WW-fusion events and  $\epsilon_{ZH} = 0.422$  is the efficiency on Higgs-Strahlung events. A determination of relative uncertainty  $\sigma_{WW}$  is given to be 32 % in Section 2.3. The results of the fit are listed in Table 2.3.

**Table 2.3:** Statistical fitting uncertainty branching ratio times production cross section and in the lower part uncertainty of branching ratio using template fit; the branching ratio to bottom quarks can not measured with the here described method.

| optimized on   | $h \rightarrow b\bar{b}$ | $h \rightarrow c\bar{c}$ | $h \rightarrow gg$ | $h \rightarrow b\bar{b}, c\bar{c}, gg$ |
|--|--------------------------|--------------------------|--------------------|--|
| $\frac{\Delta(\sigma \cdot BR(h \rightarrow b\bar{b}))}{\sigma \cdot BR_{SM}(h \rightarrow b\bar{b})}$ | 1.81 %                   | 2.62 %                   | 3.47 %             | 1.82 %                                 |
| $\frac{\Delta\sigma \cdot BR(h \rightarrow c\bar{c})}{\sigma \cdot BR_{SM}(h \rightarrow c\bar{c})}$   | 24.5 %                   | 21.54 %                  | 61.15 %            | 26.85 %                                |
| $\frac{\Delta\sigma \cdot BR(h \rightarrow gg)}{\sigma \cdot BR_{SM}(h \rightarrow gg)}$               | 16.52 %                  | 29.41 %                  | 10.05 %            | 16.15 %                                |
| $\frac{\Delta BR(h \rightarrow b\bar{b})}{BR_{SM}(h \rightarrow b\bar{b})}$                            | (4.8 %)                  | (5.2 %)                  | (5.7 %)            | (4.8 %)                                |
| $\frac{\Delta BR(h \rightarrow c\bar{c})}{BR_{SM}(h \rightarrow c\bar{c})}$                            | 25 %                     | 22 %                     | 61 %               | 27 %                                   |
| $\frac{\Delta BR(h \rightarrow gg)}{BR_{SM}(h \rightarrow gg)}$  | 17 %                     | 30 %                     | 11 %               | 17 %                                   |

## 2.2.2 TMVA

The Toolkit for Multivariate Data Analysis (TMVA) [12] is an alternative to the template fitting procedure described previously. In the following, the advantages that can be expected from using TMVA will be assessed. This can not be seen as a full study but rather as a first look at what improvement we can expect from using TMVA. The Boosted Decision Tree algorithm was found to achieve the best performance. Here the b- and c-tags of the two jets were used as input variables. As training trees for signal the same samples with 100,000 events for each final state were used as before for the templates. For testing a sample of 128,000  $\nu\bar{\nu}h$  events were used including all of the Higgs decays. For background the same samples were used for testing and training. In a full study statistical independent events should be used for testing and training. The expected uncertainties are listed in Table 2.4.

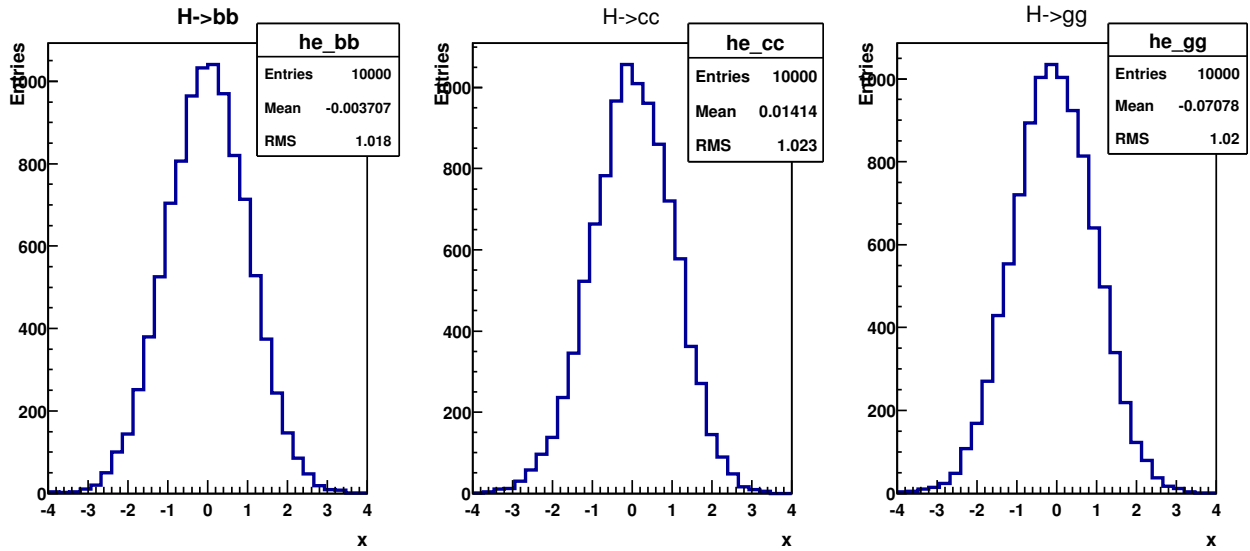


**Figure 2.1:** The results of the toy study for  $b\bar{b}$ ,  $c\bar{c}$  and  $g g$  events (from left to right), where  $x = \frac{N_{fit} - N_{SM}}{\Delta N_{fit}}$  with  $N_{SM} = \epsilon\sigma_{SM}(h\nu\bar{\nu})BR_{SM}(h \rightarrow \bar{b}b/\bar{c}c/gg)$ . The result of  $g g$  event fit has a small bias, that means some gluon events get selected as background events.

**Table 2.4:** Statistical TMVA uncertainty; the branching ratio to bottom quarks can not measured with the here described method.

| optimized on   | $h \rightarrow b\bar{b}$ | $h \rightarrow c\bar{c}$ | $h \rightarrow gg$ | $h \rightarrow b\bar{b}, c\bar{c}, gg$ |
|--|--------------------------|--------------------------|--------------------|--|
| $\frac{\Delta\sigma \cdot BR(h \rightarrow b\bar{b})}{\sigma \cdot BR_{SM}(h \rightarrow b\bar{b})}$ | 1.75 %                   |                          |                    | 1.73 %                                 |
| $\frac{\Delta\sigma \cdot BR(h \rightarrow c\bar{c})}{\sigma \cdot BR_{SM}(h \rightarrow c\bar{c})}$ |                          | 18.6 %                   |                    | 22.8 %                                 |
| $\frac{\Delta\sigma \cdot BR(h \rightarrow gg)}{\sigma \cdot BR_{SM}(h \rightarrow gg)}$             |                          |                          | 6.3 %              | 9.7 %                                  |
| $\frac{\Delta BR(h \rightarrow b\bar{b})}{BR_{SM}(h \rightarrow b\bar{b})}$                          | (4.8 %)                  |                          |                    | (4.8 %)                                |
| $\frac{\Delta BR(h \rightarrow c\bar{c})}{BR_{SM}(h \rightarrow c\bar{c})}$                          |                          | 19 %                     |                    | 23 %                                   |
| $\frac{\Delta BR(h \rightarrow gg)}{BR_{SM}(h \rightarrow gg)}$                                      |                          |                          | 7.8 %              | 11 %                                   |

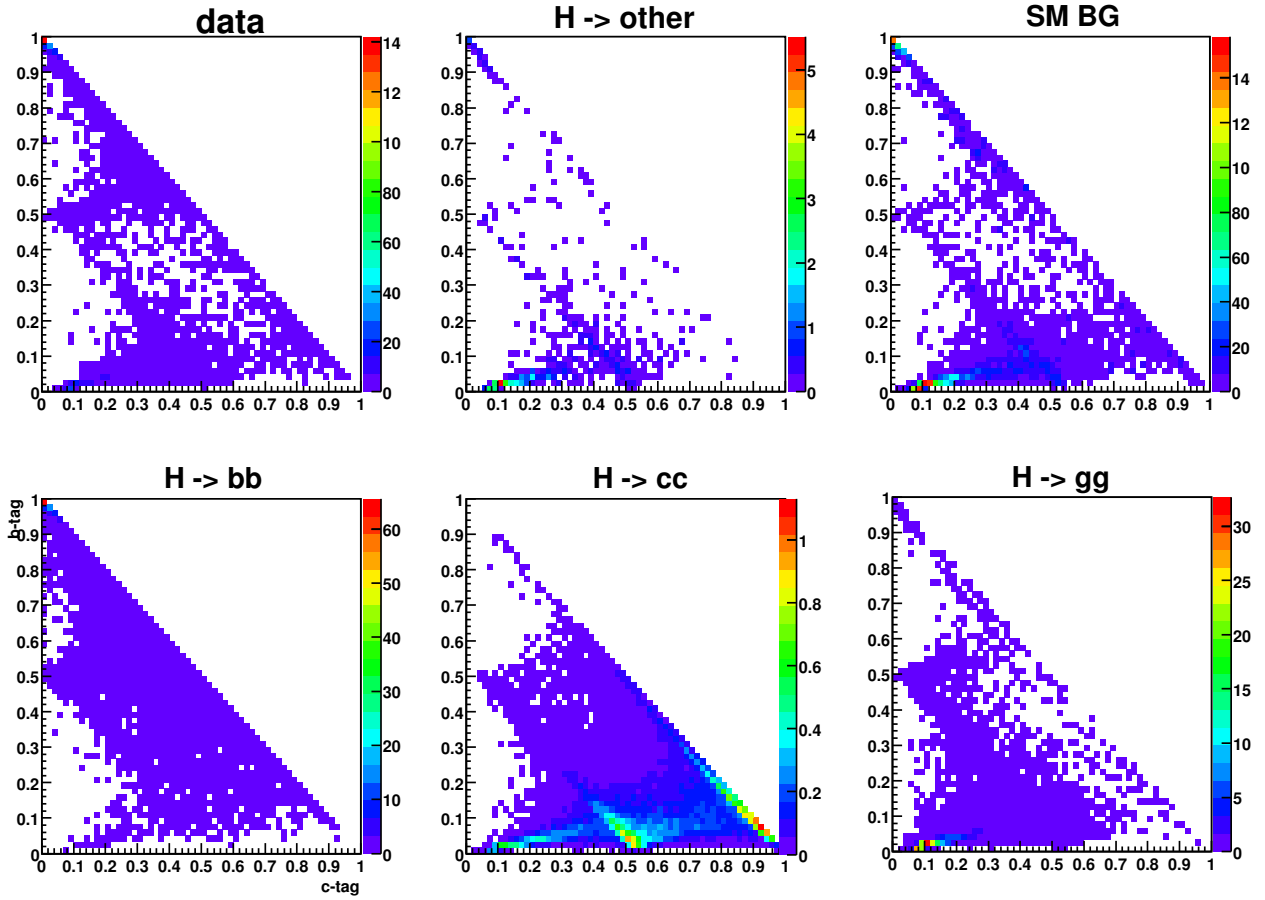


**Figure 2.2:** Two dimensional plots of  $Ph \rightarrow b\bar{b}$  versus  $Ph \rightarrow c\bar{c}$  likeness. Upper left: distribution in a typical data sample generated from the templates (lower row and upper right), these plots 100 by 100 bins resolve details. However, the fit uses 20 by 20 bins.

## 2.3 T-, S-Channel and Interference

Initially, the interference of Higgs-Strahlung (S-Channel) and WW-fusion (T-Channel) was expected to be small and thereby negligible as it was assumed in [11]. Figure A.14 clearly shows this assumption to be incorrect, since this effect does indeed affect the reconstructed Z-boson mass. While the cross section is nearly not affected.

$$\sigma(e^-e^+ \rightarrow \nu_e\bar{\nu}_e h) = 61.11 \text{ fb}^{-1}$$

$$\sigma(e^-e^+ \rightarrow \nu_\mu\bar{\nu}_\mu h) = 33.85 \text{ fb}^{-1}$$

$$\sigma_{\text{WW}}(e^-e^+ \rightarrow \nu_\mu\bar{\nu}_\mu h) = 26.34 \text{ fb}^{-1}$$

which leads to

$$\sigma_I(e^-e^+ \rightarrow \nu\bar{\nu}h) = \sigma(e^-e^+ \rightarrow \nu_e\bar{\nu}_e h) - \sigma(e^-e^+ \rightarrow \nu_\mu\bar{\nu}_\mu h) - \sigma_{\text{WW}}(e^-e^+ \rightarrow \nu_\mu\bar{\nu}_\mu h) = 0.92 \text{ fb}^{-1}$$

which is in the same order of the used cross section calculation.<sup>2</sup>

Figure A.14 illustrates that the interference is relatively high at 250 GeV. That makes the interference especially important at this energy. A comparison of the interference at higher energy shows that it decreases (see Figure A.14 or [13]). The fraction of WW-fusion and Higgs-Strahlung is more significant for 350 GeV center of mass energy and at 500 GeV the interference term can be neglected. The ratio of Higgs-Strahlung and WW-fusion is not trivial and model dependent. Consequently, the long-term goal is to measure each term independently. A comparison to simulated data may help to reach this goal. Alternatively, fitting the recoil mass from other channels to the considered one in order to ensure independence of each measurement is even more promising.  $e^-e^+ \rightarrow \mu\mu h$  events could provide a template for Higgs-Strahlung.. In case of comparing to simulated data it would be necessary to simulate a spectrum of different Higgs to W-boson couplings. These methods are rather complex and out of the scope of this study. A template fit similar to the template fit for the branching ratio was tried, but could not be finished in time. The templates for the fit are reproduced in Figure A.15. The fit does not consider differences in the shape of the interference if the T-Channel becomes lower. Nevertheless, this is an important effect that needs to be studied in the future.

The branching ratio measurement shall serve as a first insight into the uncertainty of the production cross section via WW-fusion. Here, the cross section of WW-fusion is given by:

$$\sigma_{\text{WW}} = \frac{N_{\text{fit}}(h \rightarrow b\bar{b})}{\mathcal{L} \cdot \epsilon_{\text{WW}} \text{BR}(h \rightarrow b\bar{b})} - \frac{\epsilon_{ZH}}{\epsilon_{\text{WW}}} \sigma_{ZH}$$

<sup>2</sup>The cross sections are estimated by Whizard with a polarization of  $P(e^-, e^+) = (-100\%, 0\%)$ . Only this polarization mode was used, because WW-fusion does not occur for the opposite polarization.

and the relative uncertainty is given as

$$\Delta\sigma_{WW} = \sqrt{\frac{N_{fit}}{\mathcal{L}\epsilon_{WW}BR} \left( \frac{\Delta N_{fit}}{N_{fit}} + \frac{\Delta BR}{BR} \right) + \frac{\epsilon_{ZH}}{\epsilon_{WW}} \Delta\sigma_{ZH}}$$

where  $N_{fit} = N_{fit}(h \rightarrow b\bar{b})$  and  $BR = BR(h \rightarrow b\bar{b})$ ,  $\epsilon_{WW} = 0.234$  the efficiency on WW-fusion events and  $\epsilon_{ZH} = 0.422$  the efficiency on Higgs-Strahlung events. If we assume the uncertainty on the branching ratio to be 2.8 % taken from the other channels of Higgs-Strahlung from the previous study [14]<sup>3</sup> and uncertainty on the cross section of Higgs-Strahlung as 2.5% [2]. The error on the cross section of WW-fusion is around 32 %, neglecting the errors for the efficiency and integrated luminosity<sup>4</sup>. We think that this error can be improved by one of the other strategies described earlier. The uncertainty is limited by the number of WW-fusion to bottom quark pairs by 1.72 % if assuming perfect selection of signal. But if we guess more realistically a purity of 0.5 and signal efficiency of 0.3 the relative uncertainty on the cross section of Higgs production via WW-fusion would be 5.7 %. This would lead to an uncertainty of the branching ratio to bottom quark from the template fit of  $\frac{\Delta BR(h \rightarrow b\bar{b})}{BR(h \rightarrow b\bar{b})} = 2.9\%$ .

## 2.4 Hadronic Beam-Background

Photons from the beam can annihilate to quark pairs. This process is predicted by the Detailed Baseline Design [5] to a mean of 0.4 per bunch crossing. However, in the samples used for this study a mean of 0.2 was overlaid in the samples used for this study on the events. That is why it is important to investigate how the analysis is affected by this beam-background. Therefore, additional signal data samples with no overlay and samples with a mean of 0.4 were generated. The background samples could not be generated under these conditions, because it would consume too much time. To check the influence on the template fit a MC toy study was performed with the template from the samples with different distributions of beam-background, where the background sample stayed the same. Hereby, the results were found to remain the same within statistical uncertainties (see Table 2.5). Hence, the beam background is expected to have only minimal impact on the flavor tagging. Further, the influence on the event selection was studied. As there are no background samples available with different means of overlaid background, we scaled the events with overlay to the respective number of overlay in all samples. Not all overlay is clustered to the jets and is contributing to the event selection. The overlay can be just not detected or not selected by the jet finder. The scale factor for an event without overlay was chosen to  $s_{no}^{\mu_1 \rightarrow \mu_2} = \frac{N_{no}^{\mu_2}/N^{\mu_2}}{N_{no}^{\mu_1}/N^{\mu_1}}$  to make a sample

<sup>3</sup>In this study a Higgs-mass of 120 GeV is promised. That means that the Higgs-Strahlung production cross section and the branching ratio Higgs to bottom pair is lower at 125 GeV Higgs-mass since the flavor-tagging improved. The uncertainty is assumed to be of the same order.

<sup>4</sup>The integrated luminosity can be measured to an uncertainty of 4.3 per mil [7], which is nowhere near the here calculated uncertainties.



**Table 2.5:** Results of the toy study with different mean of hadronic beam-background per bunch crossing

| overlay mean                             | $\mu = 0$ | $\mu = 0.2$ | $\mu = 0.4$ |
|--|-----------|-------------|-------------|
| $N_{fit}(h \rightarrow b\bar{b})$        | 4248      | 4248        | 4248        |
| $\Delta N_{fit}(h \rightarrow b\bar{b})$ | 76.5      | 77.4        | 77.26       |
| $N_{fit}(h \rightarrow c\bar{c})$        | 192.7     | 193.3       | 193.5       |
| $\Delta N_{fit}(h \rightarrow c\bar{c})$ | 50.96     | 51.91       | 51.23       |
| $N_{fit}(h \rightarrow gg)$              | 469       | 470         | 470         |
| $\Delta N_{fit}(h \rightarrow gg)$       | 72.8      | 75.88       | 70.38       |

with mean  $\mu_1$  similar to a sample with mean  $\mu_2$ . In the same sense an event with overlay was scaled with  $s_{with}^{\mu_1 \rightarrow \mu_2} = \frac{N_{with}^{\mu_2}/N^{\mu_2}}{N_{with}^{\mu_1}/N^{\mu_1}}$ , where  $N^{\mu_1}$  is the total number of events in the sample and  $N_{with}^{\mu_1}, N_{no}^{\mu_1}$  the number with and without overlay. In the case of scaling from  $\mu_1 = 0.2$  to  $\mu_2 = 0.4$  the events with one overlaid event are overestimated by 11 % and with two overlaid events underestimated by 44 %. Since events with one or zero overlaid events make up 93.8 % of all events <sup>5</sup> this assumption is reasonable. Optimizing the cuts once again the significance changes as listed in Table 2.6. If a mean of 0.4 overlaid background events at

**Table 2.6:** Significance for different mean of hadronic beam-background per bunch crossing

| overlay mean | $\mu = 0$ | $\mu = 0.2$ | $\mu = 0.4$ |
|--------------|-----------|-------------|-------------|
| significance | 53.37     | 51.87       | 50.79       |

ILC is assumed, the significance will go down by just a little bit over 2 %. The effect could get enhanced by the template fit, but will not influence the estimated error by more than 5 %.

<sup>5</sup>Adding events with two overlaid events, the contribution is 99,2 %. In real data it is even more, because not all overlay gets selected.



# 3 Summary and Outlook

The accuracies of the Higgs branching ratio times production cross section ( $\Delta(\sigma \cdot BR)/(\sigma \cdot BR)$ ) to bottom, charm quark pair and gluons could be estimated to be 1.8 %, 22 % and 10 % using a template fit. We improved the measurement for gluon and charm quark final state by optimizing the event selection only on one final state at a time. The accuracy on the branching ratio to charm quarks is rather high. This may be an effect due to flavor tagging, but it needs further investigation. We found the Toolkit for Multivariate Data Analysis to be a worthwhile way to improve the branching ratio measurement. Even at a mean of 0.4 the hadronic beam-background was found to have a minor influence on the branching ratio study.

A first attempt at measuring the production cross section of  $\nu\bar{\nu}h$  via WW-fusion WW-fusion yielded a value to 32 % using the branching ratio to bottom pair measurement. A direct measurement will certainly improve this result and make the measurement of the branching ratio to bottom quarks possible. Further, the interference of WW-fusion and Higgs-Strahlung is promising and needs further investigation.

The relative uncertainty of the Higgs branching ratio ( $\Delta BR/BR$ ) to  $c\bar{c}$  and  $gg$  was estimated to be 22 % and 11 % assuming  $\Delta\sigma_{WW}/\sigma_{WW} = 32\%$  and  $\Delta\sigma_{ZH}/\sigma_{ZH} = 2.5\%$  from Z-boson recoil mass measurement.



## 4 Bibliography

- [1] Georges Aad et al. Observation of a new particle in the search for the Standard Model Higgs boson with the ATLAS detector at the LHC. *Phys.Lett.*, B716:1–29, 2012.
- [2] Toshinori Abe et al. The International Large Detector: Letter of Intent. 2010.
- [3] I. Antcheva, M. Ballintijn, B. Bellenot, M. Biskup, R. Brun, et al. ROOT: A C++ framework for petabyte data storage, statistical analysis and visualization. *Comput.Phys.Commun.*, 182:1384–1385, 2011.
- [4] D. Bailey et al. The LCFIVertex package: vertexing, flavour tagging and vertex charge reconstruction with an ILC vertex detector. *Nucl.Instrum.Meth.*, A610:573–589, 2009.
- [5] Ties Behnke, James E. Brau, Philip N. Burrows, Juan Fuster, Michael Peskin, et al. The International Linear Collider Technical Design Report - Volume 4: Detectors. 2013.
- [6] Ties Behnke, James E. Brau, Brian Foster, Juan Fuster, Mike Harrison, et al. The International Linear Collider Technical Design Report - Volume 1: Executive Summary. 2013.
- [7] I. Bozovic-Jelisavcic, S. Lukic, M. Pandurovic, and I. Smiljanic. Precision luminosity measurement at ILC. 2014.
- [8] S. Brandt, C. Peyrou, R. Sosnowski, and A. Wroblewski. The Principal axis of jets. An Attempt to analyze high-energy collisions as two-body processes. *Phys.Lett.*, 12:57–61, 1964.
- [9] Matteo Cacciari, Gavin P. Salam, and Gregory Soyez. FastJet User Manual. *Eur.Phys.J.*, C72:1896, 2012.
- [10] Serguei Chatrchyan et al. Observation of a new boson at a mass of 125 GeV with the CMS experiment at the LHC. *Phys.Lett.*, B716:30–61, 2012.
- [11] Claude Dürig, Keisuke Fujii, Jenny List, and Junping Tian. Model Independent Determination of  $HWW$  coupling and Higgs total width at ILC. 2014.
- [12] Andreas Hocker, J. Stelzer, F. Tegenfeldt, H. Voss, K. Voss, et al. TMVA - Toolkit for Multivariate Data Analysis. *PoS*, ACAT:040, 2007.

- 
- [13] W Kilian, M Kramer, and P.M. Zerwas. Higgsstrahlung and W W fusion in  $e^+ e^-$  collisions. *Phys.Lett.*, B373:135–140, 1996.
  - [14] Hiroaki Ono and Akiya Miyamoto. A study of measurement precision of the Higgs boson branching ratios at the International Linear Collider. *Eur.Phys.J.*, C73:2343, 2013.
  - [15] M.A. Thomson. Particle Flow Calorimetry and the PandoraPFA Algorithm. *Nucl.Instrum.Meth.*, A611:25–40, 2009.
  - [16] Wouter Verkerke and David Kirkby. [roofit.sourceforge.net](https://github.com/rofit).
  - [17] O. Wendt, F. Gaede, and T. Kramer. Event Reconstruction with MarlinReco at the ILC. *Pramana*, 69:1109–1114, 2007.

# A Appendix

## A.1 Event selection

In the following plots of the cut variables are shown. The vertical line indicates the cut limit for all final states optimized together. Each of the shown distribution is scaled to one. The signal is shown without any cut, while the background is shown with all cut but without the cut limit on the variable shown.

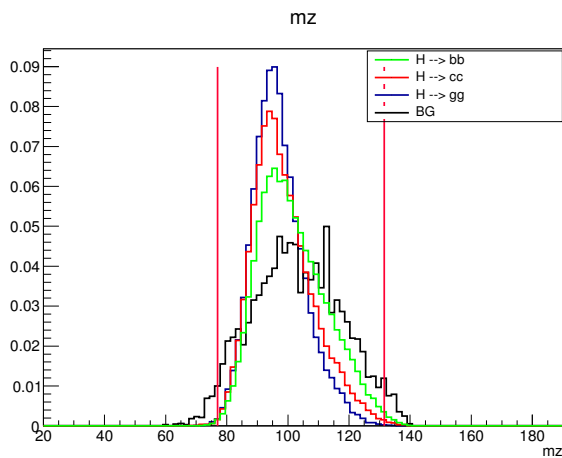


**Figure A.1:**  $M_Z$ ; for gluon and charm quark the limit can be tighter.

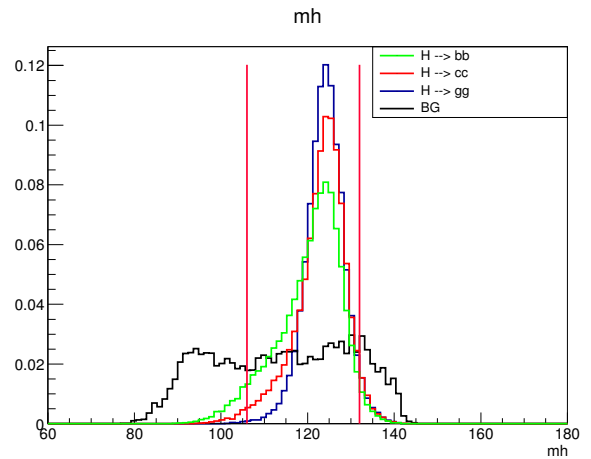


**Figure A.2:**  $M_H$ ; the distribution from ZZ processes with one invisible Z-boson is easily to spot, the lower limit can be tighter for charm and gluon final states.

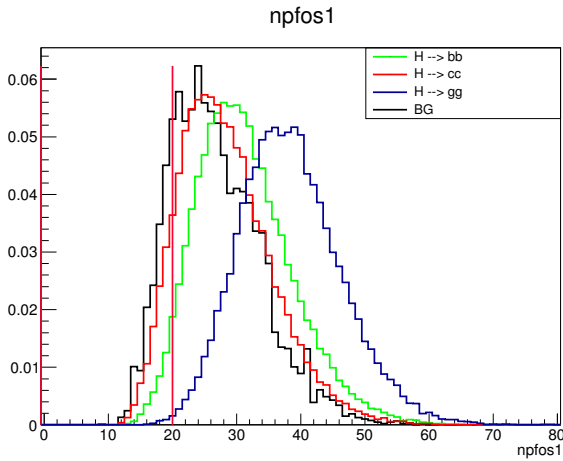


**Figure A.3:**  $N_{PFO,1}$ ; limit should be higher for  $c\bar{c}$  and gg. An upper limit is not needed.

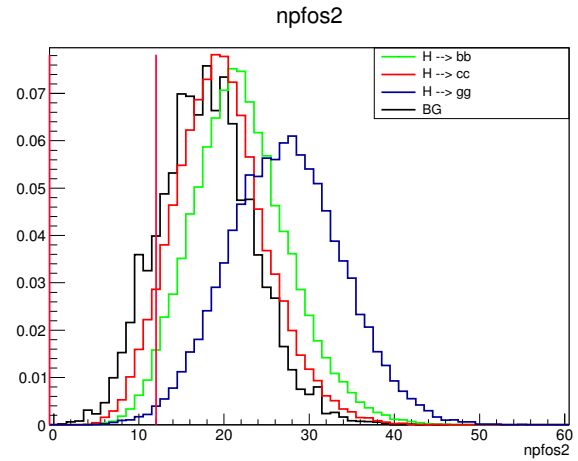


**Figure A.4:**  $N_{PFO,2}$ ; limit should be higher for  $c\bar{c}$  and gg. An upper limit is not needed.

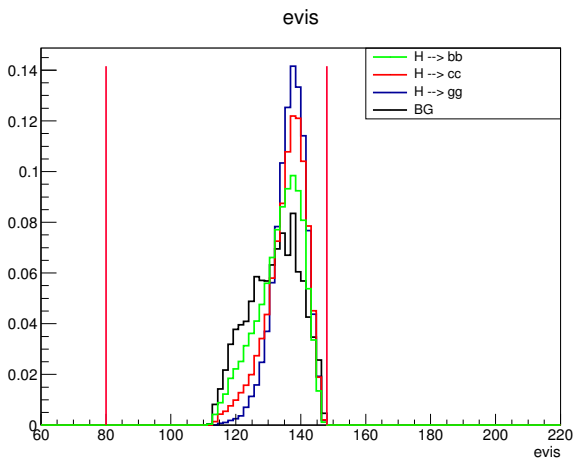


**Figure A.5:**  $E_{vis}$ ; in this optimization mode this cut does not reduce background, but for gluon a cut can be useful.

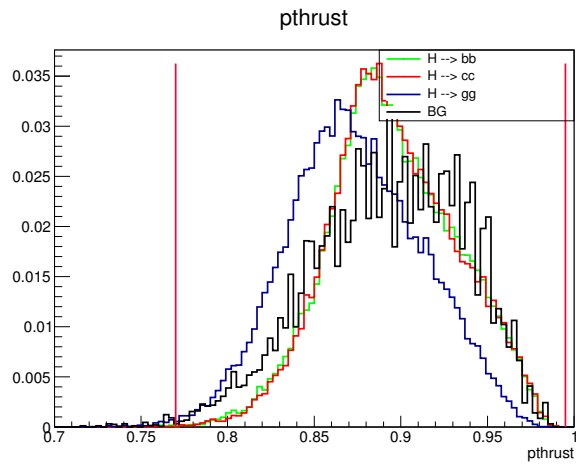


**Figure A.6:** principle thrust; does not cut much background but if it is optimized on gluons the upper limit cuts background and for charm final state the lower limit.

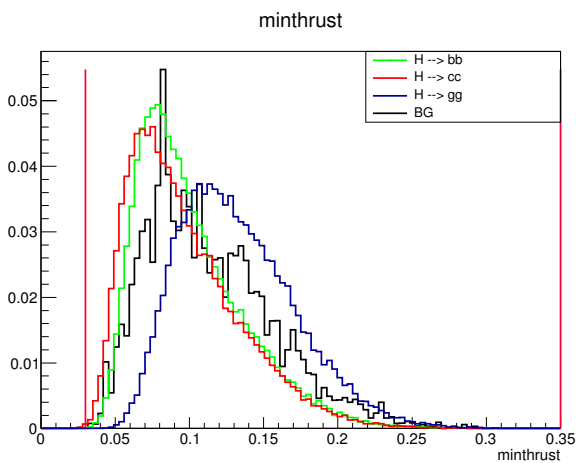


**Figure A.7:** minimal thrust; this variable only reduces background for charm final state.

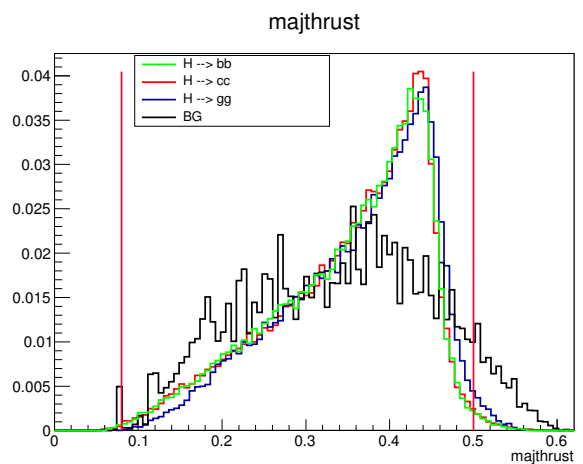


**Figure A.8:** major thrust; can be tighter for gluon final state.



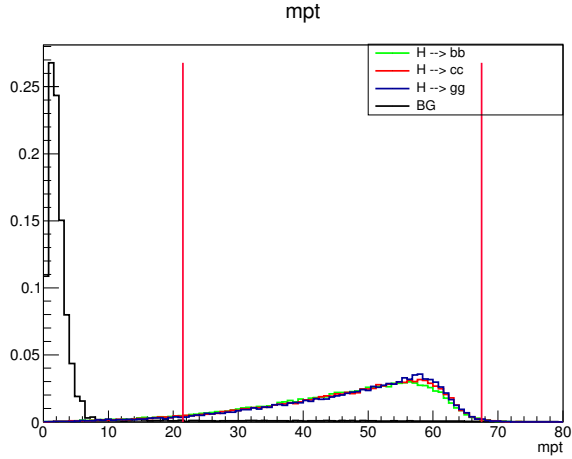


**Figure A.9:**  $p_{mis,t}$ ; important cut to reduce  $q\bar{q}$ , to reach a higher WW-fusion efficiency this cut should be looser.

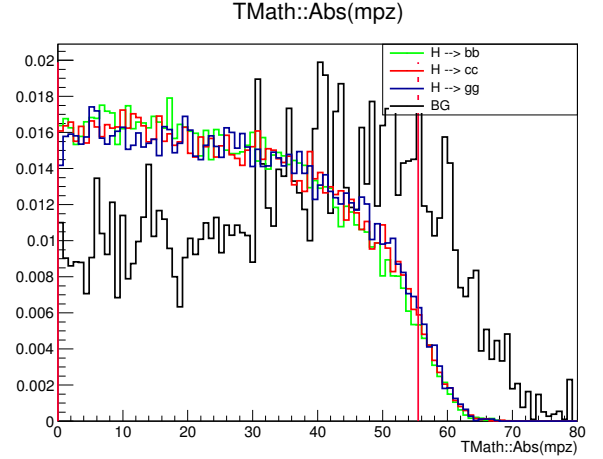


**Figure A.10:**  $|p_{mis,z}|$ ; to reach a higher WW-fusion efficiency this cut should be looser.

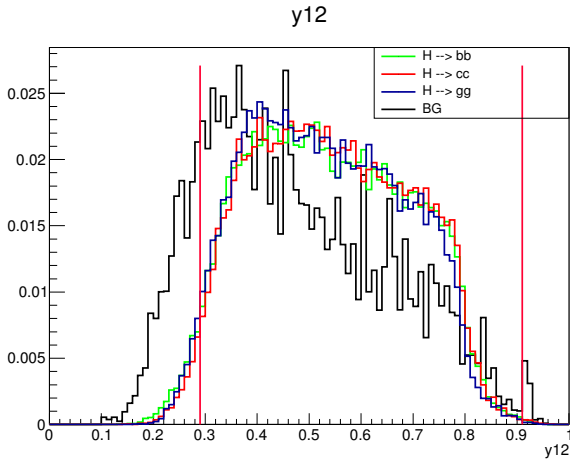


**Figure A.11:**  $Y_{12}$ ; looks very similar for signal since they all two jet final states.

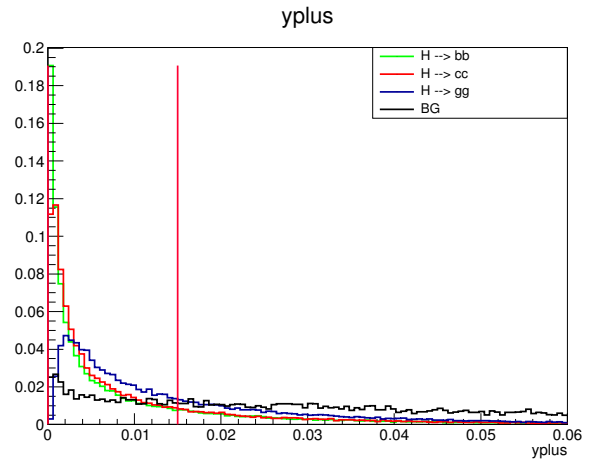


**Figure A.12:**  $Y_{23}$ ; is especially important to cut  $q\bar{q}\nu\ell$  background.

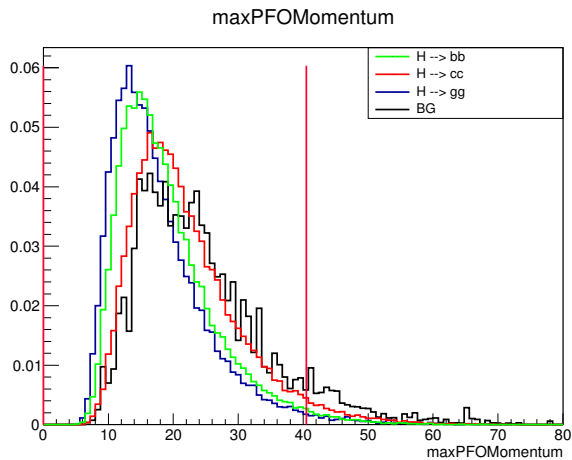


**Figure A.13:**  $p_{max,PFO}$ ; upper limit can be tighter for gluon final states, lower limit is not needed.

**Table A.1:** Background reduction for optimizing on  $h \rightarrow b\bar{b}, c\bar{c}, gg$ ; the cut limits can be found in Table A.3, other BG include minijet events and processes triggered by beam photons

|                       | $\nu\bar{\nu}h(\text{fusion})$ | $\nu\bar{\nu}h(\text{ZH})$ | $\nu\bar{\nu}b\bar{b}$ | $\nu\bar{\nu}q\bar{q}$ | $q\bar{q}\ell\bar{\ell}$ | $q\bar{q}\ell\nu$ | $q\bar{q}q\bar{q}$ | $q\bar{q}$        | leptonic          | Higgs             | other             | Significance | Purity               | Efficiency |
|-----------------------|--------------------------------|----------------------------|------------------------|------------------------|--------------------------|-------------------|--------------------|-------------------|-------------------|-------------------|-------------------|--------------|----------------------|------------|
| Expected              | 3960                           | $1.54 \cdot 10^4$          | $3.31 \cdot 10^4$      | $1.26 \cdot 10^5$      | $2.18 \cdot 10^5$        | $4.22 \cdot 10^6$ | $4.20 \cdot 10^6$  | $1.95 \cdot 10^7$ | $1.06 \cdot 10^7$ | $6.04 \cdot 10^4$ | $4.72 \cdot 10^8$ | 0.592        | $2.62 \cdot 10^{-5}$ | 1          |
| isolEPCuts            | 3620                           | $1.40 \cdot 10^4$          | $3.28 \cdot 10^4$      | $1.26 \cdot 10^5$      | $9.40 \cdot 10^4$        | $1.53 \cdot 10^6$ | $4.17 \cdot 10^6$  | $1.92 \cdot 10^7$ | $2.38 \cdot 10^6$ | $5.11 \cdot 10^4$ | $3.34 \cdot 10^8$ | 0.697        | $3.66 \cdot 10^{-5}$ | 0.992      |
| $N_{PFO}$             | 3020                           | $1.17 \cdot 10^4$          | $2.64 \cdot 10^4$      | $7.08 \cdot 10^4$      | $5.04 \cdot 10^4$        | $7.00 \cdot 10^5$ | $4.04 \cdot 10^6$  | $1.22 \cdot 10^7$ | 2730              | $4.97 \cdot 10^4$ | $2.06 \cdot 10^6$ | 2.77         | $6.32 \cdot 10^{-4}$ | 0.907      |
| $E_{vis}$             | 2450                           | $1.09 \cdot 10^4$          | $2.55 \cdot 10^4$      | $6.84 \cdot 10^4$      | $1.23 \cdot 10^4$        | $3.02 \cdot 10^5$ | 334                | $4.91 \cdot 10^6$ | 630               | 671               | $1.23 \cdot 10^6$ | 4.33         | $1.69 \cdot 10^{-3}$ | 0.829      |
| $M_Z$                 | 1940                           | $1.01 \cdot 10^4$          | $1.98 \cdot 10^4$      | $5.63 \cdot 10^4$      | 3870                     | $1.42 \cdot 10^5$ | 196                | $8.58 \cdot 10^5$ | 333               | 616               | $4.54 \cdot 10^5$ | 8.1          | $6.51 \cdot 10^{-3}$ | 0.753      |
| $M_H$                 | 1730                           | 9240                       | 1600                   | 5820                   | 1530                     | $6.26 \cdot 10^4$ | 94.7               | $6.35 \cdot 10^4$ | 185               | 370               | $1.86 \cdot 10^5$ | 16           | 0.028                | 0.69       |
| missMo_t              | 1370                           | 8440                       | 1220                   | 4330                   | 613                      | $4.41 \cdot 10^4$ | 2.99               | 1640              | 30.5              | 314               | 2360              | 32.5         | 0.128                | 0.616      |
| $P_{z,mis}$           | 1240                           | 8210                       | 1000                   | 3330                   | 504                      | $3.01 \cdot 10^4$ | 2.99               | 1110              | 23.1              | 303               | 2070              | 36.3         | 0.166                | 0.594      |
| cosTHiggs             | 1240                           | 8210                       | 1000                   | 3330                   | 504                      | $3.01 \cdot 10^4$ | 2.99               | 1110              | 23.1              | 303               | 2070              | 36.3         | 0.166                | 0.594      |
| $N_\mu$               | 1240                           | 8210                       | 1000                   | 3330                   | 504                      | $3.01 \cdot 10^4$ | 2.99               | 1110              | 23.1              | 303               | 2070              | 36.3         | 0.166                | 0.594      |
| mlthrust              | 1080                           | 7290                       | 724                    | 2440                   | 304                      | $1.82 \cdot 10^4$ | 0.132              | 1000              | 19.2              | 201               | 1460              | 40.6         | 0.225                | 0.549      |
| pthrust               | 985                            | 6610                       | 625                    | 2170                   | 235                      | $1.48 \cdot 10^4$ | 0                  | 972               | 19.2              | 147               | 1230              | 41.8         | 0.251                | 0.521      |
| minthrust             | 985                            | 6610                       | 624                    | 2170                   | 235                      | $1.48 \cdot 10^4$ | 0                  | 972               | 19.2              | 147               | 1220              | 41.8         | 0.251                | 0.521      |
| $P_{max,PFO}$         | 969                            | 6480                       | 593                    | 2010                   | 226                      | $1.36 \cdot 10^4$ | 0                  | 914               | 8.05              | 143               | 1140              | 42.4         | 0.263                | 0.512      |
| $Y_{12}$ and $Y_{12}$ | 617                            | 4380                       | 276                    | 973                    | 56.2                     | 2040              | 0                  | 630               | 0                 | 43.7              | 382               | 50.7         | 0.523                | 0.367      |

**Table A.2:** Results for excluding the respective cut for optimizing on  $h \rightarrow b\bar{b}, c\bar{c}, gg$ ; the cut limits can be found in Table A.3, other BG includes minijet events and processes triggered by beam photons.

|                       | fusion(Sig) | ZH(Sig) | fusion(OTHER) | ZH(OTHER) | $\nu\bar{\nu}b\bar{b}$ | $\nu\bar{\nu}q\bar{q}$ | $q\bar{q}\ell\bar{\ell}$ | $q\bar{q}\ell\nu$ | $q\bar{q}q\bar{q}$ | $q\bar{q}$ | leptonic | Higgs | other | Significance | Purity | Efficiency |
|-----------------------|-------------|---------|---------------|-----------|------------------------|------------------------|--------------------------|-------------------|--------------------|------------|----------|-------|-------|--------------|--------|------------|
| all cuts              | 608         | 4300    | 8.51          | 72.6      | 276                    | 973                    | 56.2                     | 2040              | 0                  | 630        | 0        | 43.7  | 382   | 50.7         | 0.523  | 0.367      |
| $N_{PFO}$             | 662         | 4680    | 8.06          | 83.1      | 310                    | 1410                   | 75.1                     | 3180              | 0                  | 868        | 227      | 52.7  | 558   | 48.6         | 0.441  | 0.4        |
| $E_{vis}$             | 608         | 4310    | 8.51          | 72.6      | 276                    | 973                    | 56.2                     | 2050              | 0                  | 630        | 0        | 43.7  | 382   | 50.7         | 0.522  | 0.367      |
| $M_Z$                 | 646         | 4360    | 9.57          | 73.1      | 287                    | 1010                   | 59.3                     | 2300              | 0                  | 652        | 0        | 44.6  | 419   | 50.4         | 0.507  | 0.374      |
| $M_H$                 | 661         | 4580    | 10.4          | 81.3      | 656                    | 2150                   | 72.4                     | 3160              | 0                  | 1250       | 0        | 64.8  | 1050  | 44.8         | 0.382  | 0.392      |
| missMo_t              | 734         | 4550    | 9.61          | 76.9      | 327                    | 1170                   | 138                      | 2590              | 5.08               | 10700      | 27       | 49.2  | 90800 | 15.8         | 0.0475 | 0.395      |
| $P_{z,mis}$           | 655         | 4420    | 8.52          | 76.2      | 313                    | 1120                   | 61.6                     | 2540              | 0                  | 803        | 0        | 44.4  | 401   | 49.6         | 0.486  | 0.379      |
| cosTHiggs             | 608         | 4300    | 8.51          | 72.6      | 276                    | 973                    | 56.2                     | 2040              | 0                  | 630        | 0        | 43.7  | 382   | 50.7         | 0.523  | 0.367      |
| $N_\mu$               | 608         | 4300    | 8.51          | 72.6      | 276                    | 973                    | 56.2                     | 2040              | 0                  | 630        | 0        | 43.7  | 382   | 50.7         | 0.523  | 0.367      |
| mlthrust              | 631         | 4350    | 9.7           | 76.2      | 316                    | 1110                   | 62.7                     | 2170              | 0                  | 663        | 0        | 51.3  | 405   | 50.2         | 0.505  | 0.372      |
| pthrust               | 610         | 4310    | 8.93          | 74.9      | 278                    | 979                    | 57.4                     | 2050              | 0                  | 630        | 0        | 44.8  | 384   | 50.7         | 0.522  | 0.368      |
| minthrust             | 608         | 4310    | 8.51          | 72.6      | 276                    | 974                    | 56.2                     | 2040              | 0                  | 630        | 0        | 43.7  | 382   | 50.7         | 0.523  | 0.367      |
| $P_{max,PFO}$         | 617         | 4390    | 9.11          | 74.4      | 288                    | 1050                   | 57.4                     | 2310              | 0                  | 652        | 1.44     | 45.2  | 412   | 50.3         | 0.506  | 0.374      |
| $Y_{12}$ and $Y_{12}$ | 889         | 5960    | 80            | 520       | 593                    | 2010                   | 226                      | 13600             | 0                  | 914        | 8.05     | 143   | 1140  | 42.4         | 0.263  | 0.512      |

In Table A.2 are cuts, which have very small or no influence on significance, but these cuts can become more important if it is optimized on only one of the decay mode. Since they do not have negative effect and by reason of simplicity, all cuts were always included.

**Table A.3:** An overview of all cut variables optimized to different final states.  $S_{xx}$  stands for  $\frac{N(\text{h} \rightarrow xx)}{\sqrt{N(\text{h} \rightarrow xx) + N(\text{other})}}$

| optimized on    | h $\rightarrow$ b $\bar{\text{b}}$ | h $\rightarrow$ c $\bar{\text{c}}$ | h $\rightarrow$ gg | h $\rightarrow$ b $\bar{\text{b}}$ , c $\bar{\text{c}}$ , gg |
|-----------------|------------------------------------|------------------------------------|--------------------|--|
| $N_{PFO,1} >$   | 20                                 | 14                                 | 30                 | 20   |
| $N_{PFO,2} >$   | 11                                 | 9                                  | 23                 | 11   |
| $E_{vis} <$     | 147                                | 145                                | 145                | 147  |
| $E_{vis} >$     | 80                                 | 80                                 | 125                | 80   |
| $p_{max,PFO} <$ | 40.5                               | 42.5                               | 26.5               | 40.5   |
| $M_Z <$         | 131.5                              | 107.5                              | 123.5              | 131.5  |
| $M_Z >$         | 81.5                               | 82                                 | 83                 | 79.5   |
| $M_H >$         | 104.5                              | 117                                | 117.5              | 104.5  |
| $M_H <$         | 132                                | 129                                | 130                | 132  |
| $p_{t,mis} <$   | 66.5                               | 66.5                               | 68                 | 67.5   |
| $p_{t,mis} >$   | 25.5                               | 34                                 | 21                 | 21.5   |
| $ p_{z,mis}  <$ | 55                                 | 49                                 | 57                 | 55.5   |
| majthrust <     | 0.5                                | 0.48                               | 0.56               | 0.5  |
| majthrust >     | 0.08                               | 0.15                               | 0                  | 0.08   |
| pthrust >       | 0.8                                | 0.83                               | 0.64               | 0.77   |
| pthrust <       | 0.99                               | 0.985                              | 0.975              | 0.995  |
| minthrust <     | 0.35                               | 0.3                                | 0.47               | 0.35   |
| minthrust >     | 0                                  | 0                                  | 0.09               | 0.03   |
| $N_\mu <$       | 4                                  | 3                                  | 1                  | 4  |
| $Y_{12} >$      | 0.29                               | 0.285                              | 0                  | 0.29   |
| $Y_{12} <$      | 0.955                              | 0.885                              | 0.96               | 0.91   |
| $Y_{23} <$      | 0.015                              | 0.005                              | 0.055              | 0.015  |
| Significance    | 50.6                               | 38.3                               | 32                 | 50.7   |
| Efficiency      | 0.347                              | 0.137                              | 0.111              | 0.367  |
| Purity          | 0.551                              | 0.803                              | 0.689              | 0.523  |
| $S_{b\bar{b}}$  | 43.8                               | 33.8                               | 21.3               | 43.8   |
| $S_{c\bar{c}}$  | 1.95                               | 1.81                               | 0.655              | 1.97   |
| $S_{gg}$        | 4.79                               | 2.7                                | 9.97               | 4.89   |

## A.2 Data Samples

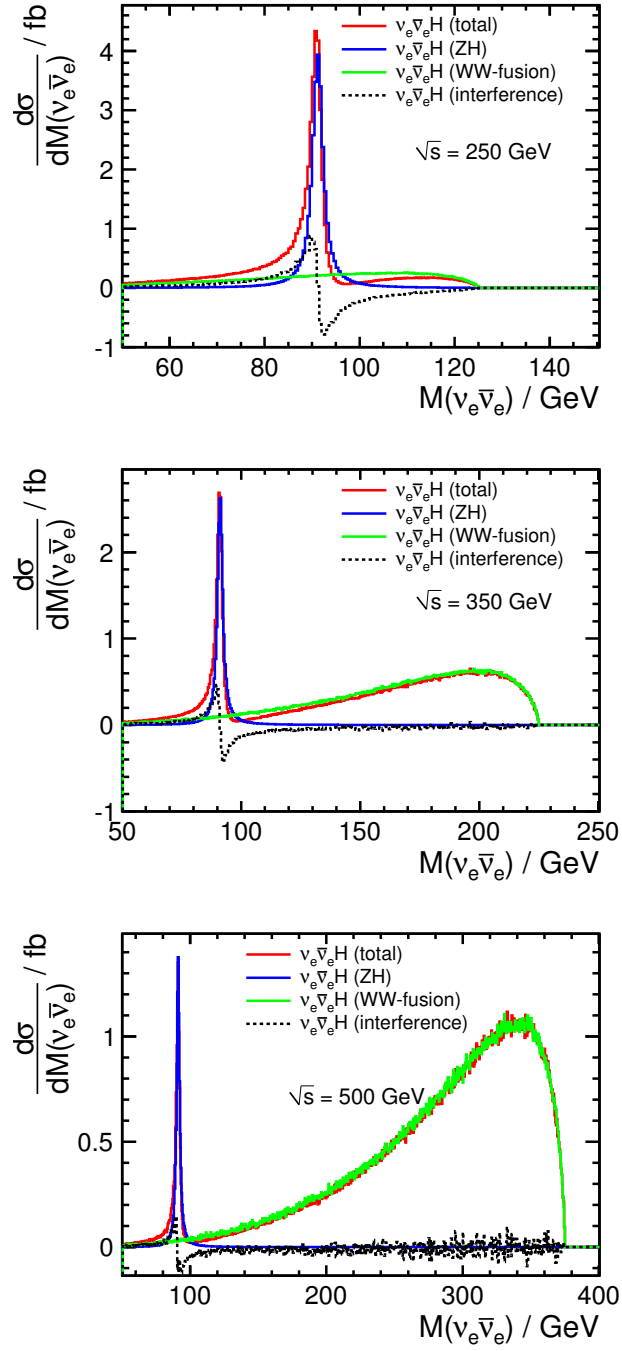
| process   | mode | expected          | generated         | after  |
|-----------|------|-------------------|-------------------|--------|
| Signal    | LR   | $1.88 \cdot 10^4$ | $1.29 \cdot 10^5$ | 4830   |
|           | RL   | $5.70 \cdot 10^2$ | $6.51 \cdot 10^4$ | 161    |
| ZZ-fusion | LR   | $6.68 \cdot 10^4$ | $1.15 \cdot 10^5$ | 498    |
|           | RL   | $1.14 \cdot 10^3$ | $3.30 \cdot 10^4$ | 5.24   |
| single W  | LL   | $9.43 \cdot 10^3$ | $3.00 \cdot 10^4$ | 2.51   |
|           | LR   | $1.46 \cdot 10^6$ | $1.93 \cdot 10^6$ | 74.4   |
|           | RL   | $7.49 \cdot 10^2$ | $2.20 \cdot 10^4$ | 0.0341 |
|           | RR   | $1.94 \cdot 10^3$ | $3.00 \cdot 10^4$ | 0.517  |
| WW        | LR   | $2.08 \cdot 10^5$ | $3.56 \cdot 10^5$ | 791    |
|           | RL   | $6.24 \cdot 10^3$ | $1.79 \cdot 10^5$ | 12.5   |
| Z to qq   | LR   | $2.75 \cdot 10^6$ | $1.92 \cdot 10^6$ | 1970   |
|           | RL   | $1.51 \cdot 10^3$ | $4.35 \cdot 10^4$ | 0.73   |
| WW        | LR   | $1.89 \cdot 10^7$ | $1.75 \cdot 10^6$ | 627    |
|           | RL   | $6.24 \cdot 10^5$ | $1.99 \cdot 10^5$ | 3.13   |
| ZZ        | LR   | $2.18 \cdot 10^6$ | $1.07 \cdot 10^6$ | 0      |
|           | RL   | $1.19 \cdot 10^3$ | $3.46 \cdot 10^4$ | 0      |
| ZZWW Mix  | LR   | $2.05 \cdot 10^5$ | $3.51 \cdot 10^5$ | 0      |
|           | RL   | $5.29 \cdot 10^3$ | $4.00 \cdot 10^4$ | 0      |
| ZZ-fusion | LR   | $1.89 \cdot 10^2$ | $8.00 \cdot 10^3$ | 0      |
|           | RL   | $4.49 \cdot 10^2$ | $8.00 \cdot 10^3$ | 0      |
| qqH       | LR   | $2.12 \cdot 10^5$ | $2.84 \cdot 10^5$ | 0      |
|           | RL   | $2.51 \cdot 10^3$ | $1.71 \cdot 10^4$ | 0      |
| eeH       | LR   | $2.31 \cdot 10^4$ | $4.00 \cdot 10^4$ | 0      |
|           | RL   | $2.50 \cdot 10^3$ | $1.71 \cdot 10^4$ | 9.51   |
| mumuH     | LR   | $5.06 \cdot 10^4$ | $3.46 \cdot 10^5$ | 32.6   |
|           | RL   | $1.94 \cdot 10^3$ | $2.22 \cdot 10^5$ | 1.23   |
| tautauH   | LR   | $2.57 \cdot 10^3$ | $1.76 \cdot 10^4$ | 0      |
|           | RL   | $9.76 \cdot 10^1$ | $1.12 \cdot 10^4$ | 0      |

| process   | mode | expected | generated         | after             |      |
|-----------|------|----------|-------------------|-------------------|------|
| ZZ        | LR   | 1        | $4.88 \cdot 10^5$ | $3.95 \cdot 10^5$ | 0    |
|           | RL   |          | $9.61 \cdot 10^1$ | $1.10 \cdot 10^4$ | 0    |
| ZW Mix    | LL   | 1        | $1.81 \cdot 10^6$ | $1.07 \cdot 10^6$ | 0    |
|           | LR   |          | $1.97 \cdot 10^3$ | $5.66 \cdot 10^4$ | 0    |
|           | RL   |          | $2.18 \cdot 10^3$ | $8.00 \cdot 10^3$ | 0    |
|           | RR   |          | $1.35 \cdot 10^5$ | $1.00 \cdot 10^5$ | 0    |
| single W  | LL   | 1        | $9.59 \cdot 10^1$ | $1.10 \cdot 10^4$ | 0.37 |
|           | LR   |          | $2.82 \cdot 10^4$ | $6.00 \cdot 10^4$ | 0    |
|           | RL   |          | $8.71 \cdot 10^2$ | $3.00 \cdot 10^4$ | 0    |
|           | RR   |          | $3.15 \cdot 10^3$ | $1.00 \cdot 10^4$ | 0    |
| ZW Mix    | LL   | 1        | $6.49 \cdot 10^2$ | $1.00 \cdot 10^4$ | 0    |
|           | LR   |          | $1.89 \cdot 10^2$ | $8.00 \cdot 10^3$ | 0    |
|           | RL   |          | $2.55 \cdot 10^2$ | $1.00 \cdot 10^4$ | 0    |
|           | RR   |          | $2.18 \cdot 10^3$ | $8.00 \cdot 10^3$ | 0    |
| eeZ       | LL   | 1        | $4.49 \cdot 10^2$ | $8.00 \cdot 10^3$ | 0    |
|           | LR   |          | $7.95 \cdot 10^4$ | $1.48 \cdot 10^5$ | 0    |
|           | RL   |          | $1.35 \cdot 10^5$ | $1.00 \cdot 10^5$ | 0    |
|           | RR   |          | $8.92 \cdot 10^3$ | $1.45 \cdot 10^5$ | 0    |
| single Z  | LR   | 1        | $1.64 \cdot 10^4$ | $1.54 \cdot 10^5$ | 0    |
|           | RL   |          | $1.59 \cdot 10^5$ | $1.74 \cdot 10^5$ | 0    |
| eeZ       | LL   | sl       | $4.21 \cdot 10^3$ | $6.47 \cdot 10^4$ | 0    |
|           | LR   |          | $2.77 \cdot 10^3$ | $7.92 \cdot 10^4$ | 0    |
|           | RL   |          | $3.10 \cdot 10^6$ | $9.00 \cdot 10^5$ | 0    |
|           | RR   |          | $1.44 \cdot 10^5$ | $7.00 \cdot 10^5$ | 0    |
| Z bha     | LL   | bha      | $6.71 \cdot 10^4$ | $1.15 \cdot 10^5$ | 0    |
|           | LR   |          | $2.05 \cdot 10^4$ | $6.59 \cdot 10^4$ | 0    |
|           | RL   |          | $3.44 \cdot 10^2$ | $2.00 \cdot 10^4$ | 0    |
|           | RR   |          | $1.98 \cdot 10^6$ | $3.00 \cdot 10^5$ | 0    |
| photon 2f | mix  | mix      | $1.10 \cdot 10^8$ | $1.79 \cdot 10^6$ | 0    |
| photon 3f | mix  | mix      | $3.61 \cdot 10^8$ | $3.95 \cdot 10^6$ | 220  |
| minijet   | mix  | mix      | $4.64 \cdot 10^6$ | $4.39 \cdot 10^5$ | 163  |

**Table A.4:** A list of data samples. In column "mode", LR denotes purely left- and right-handed electrons, l stands for leptonic, h for hadronic and sl for semileptonic. In column "process" photon 2f denotes Beam-photon reaction to two fermions. The "after" cut column shows the number of events selected as signal for optimizing on all final states together.

### A.3 T-, S-Channel and Interference



**Figure A.14:** The generated invariant neutrino mass in respect of WW-fusion, Higg-Strahlung and interference. (These plots were generated by Physim from Junping Tian.)

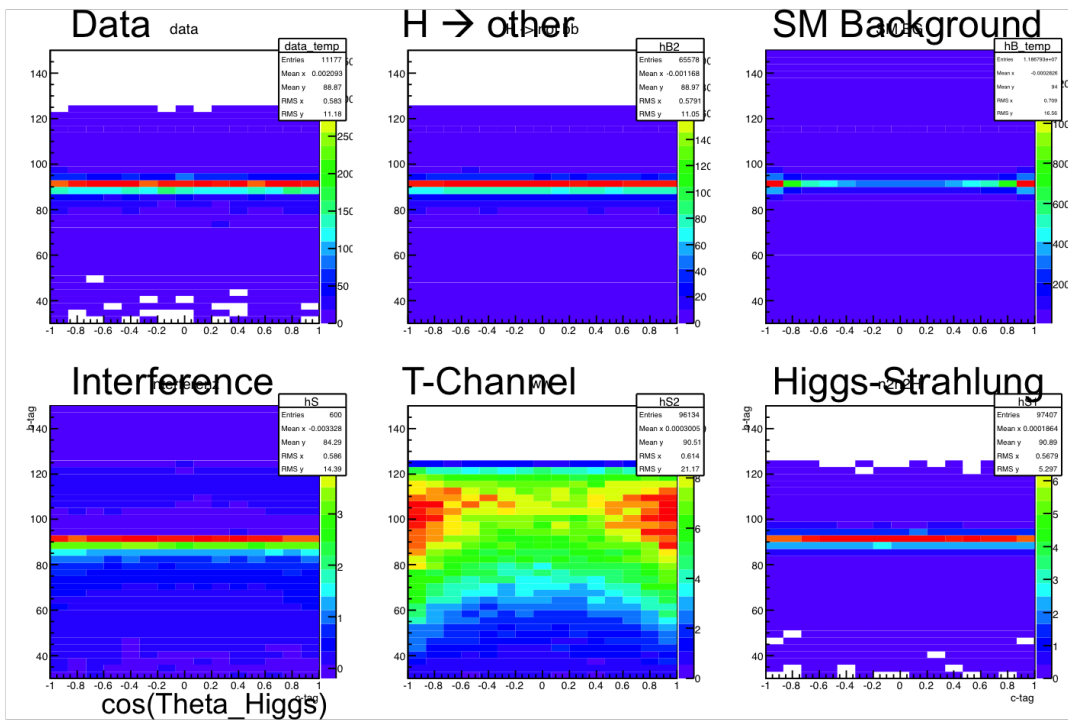


**Figure A.15:** Two dimensional plots of  $M_Z$  versus  $\cos(\Theta_H)$  where  $\Theta_H$  is the reconstructed decay angle of the Higgs-boson. Upper left: distribution in a typical data sample generated from the templates (lower row and upper right), there is still an unsolved issue with this template fit which could not be solved in time.